IOSR Journal of Engineering (IOSRJEN) **www.iosrjen.org**
ISSN (e): 2250-3021, ISSN (p): 2278-8719
PP 22-34

Half-Wave Cycloconverter-Based Photovoltaic Microinverter Topology With Phase-Shift Power Modulation

Karuna .P. Katre
Department of Electrical Engineering Abha Gaikwad Patil College of Engineering
kkatre.09@gmail.com

Abstract: *A grid-connected microinverter with a reduced num-ber of power conversion stages and fewer passive components is proposed. A high-frequency transformer and a series-resonant tank are used to interface the full-bridge inverter to the half-wave cycloconverter. All power switches are switched with zero-voltage switching. Phase-shift power modulation is used to control the out-put power of the inverter. A steady-state analysis of the proposed topology is presented to determine the average output power of the inverter. Analysis of soft switching of the full-bridge and the half-wave cycloconverter is presented with respect to voltage gain, quality factor, and phase shift of the inverter. Simulation and ex-perimental results are presented to validate the operation of the proposed topology.*

Index Terms: *Full-bridge inverter, half-wave cycloconverter, microinverter, phase-shift power modulation, series-resonant cir-cuit, zero-voltage switching (ZVS).*

I. Introduction

ENEWABLE energy has become a hot research area as **R**a result of increasing environmental issues due to fossilfuel combustion. Biomass, solar, wind, tidal, and geothermal are all potential renewable energy sources with low cost and reduced environmental effects. Solar energy plays a major role in renewable energy research as a sustainable and low environ-mental impact energy source. Among potential solar power gen-eration systems, photovoltaic (PV) systems set to grow fastest. There are four major applications of PV power generation sys-tems: off-grid domestic, off-grid non-domestic, grid-connected distributed, and grid-connected centralized [1].

The PV inverter is the key element in grid-connected PV energy systems. The main functionality of the inverter is to con-vert PV-generated dc power into grid-synchronized ac output. Grid-connected PV inverters are categorized as microinverters, string inverters, multistring inverters, mini central inverters, and central inverters [2], [3] according to the configuration of the inverter. Among these inverter configurations, the microinverter has gained popularity, as it integrates a single solar panel (50– 400 W) to the grid. Only a few years back, the cost of the overall inverter system was heavily dependent on the price of the PV module. With advancements in PV module manufacturing tech-nology and with the quantity of production, the cost of the PV module has been drastically reduced. Presently, the cost of the PV system is highly dependent on the PV inverter topology. Hence, new innovative topologies have been proposed [4]–[12] for PV microinverters with the main purpose of increasing effi-ciency and reducing the manufacturing cost. Bringing down the count of power switches by reducing the number of conversion stages is one of the key strategies to address the efficiency of the system. Also, manufacturing cost of the system can be reduced by minimizing count and size of passive components and power switches. Importantly, as the lifetime of a modern solar panel is about 25 years [13], therefore guaranteeing the reliability of the microinverter throughout its lifetime has become essential. The main strategy used to increase the reliability of the system is the removal of the electrolytic capacitors from the system where possible, because the lifetime of electrolytic capacitors reduces with elevated temperatures [14]. Also, electrolytic capacitors contribute to the overall system cost in larger percentage.

One of the first methods used to increase efficiency was to remove the high-frequency transformer at the input stage or the line frequency transformer at the output stage as in trans-formerless topologies [7]–[12]. Unfortunately, transformerless topologies need more advanced control methods or modifica-tions compared to existing topologies [11], [15], [16] to keep dc current and leakage current injection into the grid under control. Hence, there is an increased interest in grid isolated topologies as in [4]–[6] with reduced number of power conversion stages, to increase the inverter efficiency and reduce the number of passive components so as to increase the reliability of the system.

A microinverter with full-bridge inverter and a half-wave cycloconverter is proposed in [4]. Frequency modulation is used as the power control method of this inverter. Hence, it has some drawbacks such as a wide and unpredictable noise spectrum, more complex filtering of the output voltage ripple, and poor utilization of

magnetic components [17]. A dual-active-bridge-based microinverter with phase-shift modulation is proposed in [5]. Although there is a reduced number of power conversion stages as in [4], the number of power switches is increased compared to [4] due to the four quadrant switches in the output-side active bridge.

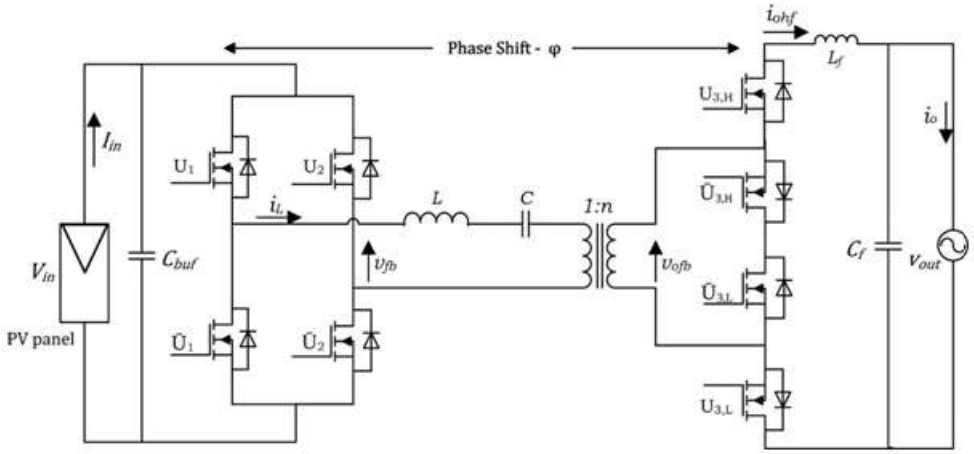

Fig. 1 Proposed microinverter topology.

In this paper, a microinverter composed of a full-bridge in-verter and a modified half-wave cycloconverter is proposed along with topological analysis and the corresponding switching strategies. The input-side full-bridge is interfaced to the output-side half-wave cycloconverter via a high-frequency transformer and a series-resonant tank, as shown in Fig. 1. All switches are switched with an identical switching frequency, which is higher than the resonant frequency of the series-resonant tank, and with a fixed duty ratio. Phase-shift power modulation is used in this topology, as proposed in [18]. The proposed topology has the following advantages:

1) the number of power switches is reduced by using sin-gle power conversion stage and by properly choosing the subsystems of the inverter;
2) the size and weight of the passive components are reduced by using a high switching frequency;
3) soft switching is used to minimize switching losses due to the higher switching frequency;
4) the leakage inductance of the transformer is used as part of the series-resonant tank to reduce the stresses on the active switches;
5) the output filter complexity is reduced by using phase-shift power modulation rather than frequency-modulated power control.

II. Topology Description And Analysis

A. Topology Description

The proposed microinverter is shown in Fig. 1. A full-bridge inverter is used to a generate three stepped (V_{in} , 0, and $-V_{\text{in}}$) symmetrical waveform from the available PV input voltage that can be considered as a constant dc voltage at the moment of interest. Although a PV generator behaves as a constant current or constant voltage source depending on its point of operation on the PV characteristic curve [19], [20], the PV input voltage can be considered as a constant dc voltage at any instant due to the availability of the buffer capacitor in the dc link and with the assumption of a slower variation in the input voltage compared to the switching frequency of the inverter [21]. A classical review of PV grid interfaces can be found in [22].

Moreover, the grid voltage can also be considered as constant over one switching cycle in the following analysis because the ratio of switching frequency f_s to grid voltage frequency f_{Vout} is very large ((f_s/f_{Vout})> 1000).

The full-bridge inverter is used as the primary-side inverter of the microinverter due to its higher voltage gain compared to the half-bridge inverter, although the number of switches in the full-bridge circuit is twice that of the half-bridge. As a consequence, the turns ratio of the high-frequency transformer can be reduced by half, and hence, the size of the transformer can be reduced. A half-wave cycloconverter is used to integrate the microinverter to the grid at the secondary side. By using a half-wave cyclo-converter, the number of switches in the secondary side can be reduced by half compared to a full-wave cycloconverter. This is expected to result in reduced switching and conduction losses in the overall inverter. In order to reduce the size of the isolation transformer, a higher switching frequency with a constant duty ratio (50%) is used to switch the power switches. As switching power loss in the active switches is proportional to the switch-ing frequency [23], zero-

voltage switching (ZVS) is used to turn ON all the switches in order to reduce turn-on switching losses. Turn-off switching power losses can be minimized by adding additional output capacitance to each power switch. ZVS is de-veloped by using the resonant nature of the series-resonant tank current in the inverter. The series-resonant tank can be placed either in the primary side, as shown in Fig. 1, or in secondary side. Placement of the series-resonant tank in the secondary side may be more advantageous considering practical aspects, such as the number of turns needed in the secondary side is higher than that in the primary side with the same inductor core. The large number of turns allows the inductor to be wound in a more accurate manner. The resonant capacitor in the series-resonant tank can be used to block any dc voltage generated by the full-bridge due to unbalanced operation. The passive filter capacitor $C_{b\ u\ f}$at the primary-side dc link is used to remove the doubleline frequency voltage and current ripple. The average size of that capacitor is in the millifarad range, and thus, electrolytic capacitors must be used as the filter. The size of the buffer capac-itor can be reduced by using a series active buffer, as proposed in [21], or by using the third ripple port, as proposed in [24].

Table I: Switching Sequence Of The Cycloconverter

		$u_{3,H}$	$u_{3,H}$	$u_{3,L}$	$u_{3,L}$
$v_{out}(+)ve$	$i_L(-)ve$	ON	OFF	OFF	ON
	$i_L(-)ve$	OFF	ON	ON	OFF
$v_{out}(-)ve$	$i_L(-)ve$	OFF	ON	ON	OFF
	$i_L(\ \ )ve$	ON	OFF	OFF	ON

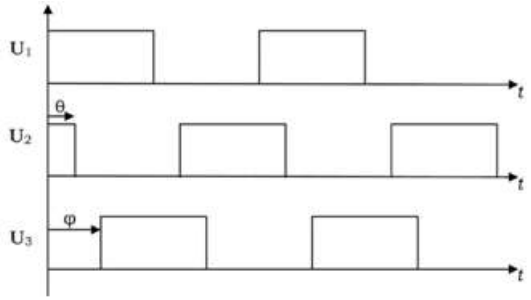

Fig. 2. Switching signals of U_1, U_2 , and U_3 .

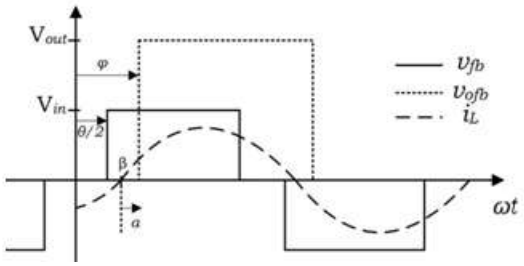

Fig. 3. Waveforms of the full-bridge, half-wave cycloconverter and resonant current when Vo u t>0.

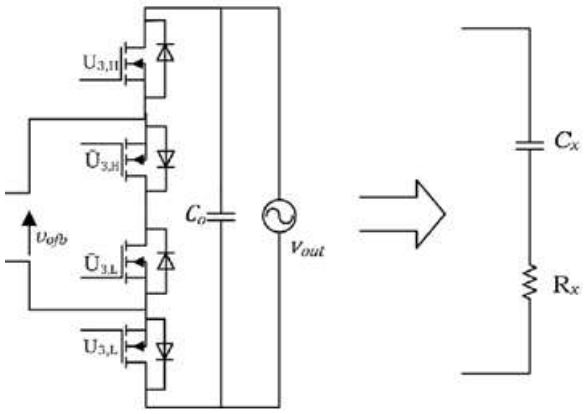

Fig. 4. Equivalent circuit of the half-wave cycloconverter.

The output filter capacitor C_f and inductor L_f in the secondary side are used to eliminate the switching frequency ripple in the output current.

B. Power Modulation

as explained in Section III-A. α is defined as $\alpha=\phi-\beta$ and β is defined as the zero crossing angle of the resonant current i_L , as shown in Fig. 3. Lower and upper bounds of α are given by

$$0 \le \alpha \le \frac{\pi}{2}. \quad (5)$$

As two bridges are connected through the inductor, there are four power modulation methods, as given in [4] and [25].

Frequency modulation in the resonant circuit causes an unpredictable noise spectrum, resulting in more complex filtering of output voltage and poor utilization of magnetic components.

Hence, phase-shift power modulation is used to control power output of this microinverter. All switches are switched using a constant fs and a fixed duty ratio (50%). fs is selected such that fs> fr , where fr is the resonant frequency of the series-resonant tank. Hence, the overall impedance seen by the fullbridge is inductive and the resonant tank current will have a lagging power factor. The switching signal of each power switch is given by (2)–(4) using the function f(.), where f(.) is defined As

$$f(x) = \begin{cases} 1, & \text{if } x \ge 0 \\ 0, & \text{otherwise.} \end{cases} \quad (1)$$

$U_1(t)$and $U_2(t)$shown in Fig. 2 are used to obtain a three step full-bridge waveform (v_{fb}), as shown in Fig. 3

$$U_1(t) = f[\sin(\omega_S t)] \quad (2)$$

$$U_2(t) = 1 - f[\sin(\omega_S t - \theta)] \quad (3)$$

$$U_3(t) = f[\sin(\omega_S t - \phi)] \; v_{out} > 0 \quad (4a)$$

$$U_3(t) = f[\sin(\omega_S t - \pi - \phi)] \; v_{out} < 0. \quad (4b)$$

The full-bridge phase-shift angle θ is given by (3) and it can be used as output voltage control variable of this microinverter, as explained in Section III-A. α is defined as $\alpha=\phi-\beta$ and β is defined as the zero crossing angle of the resonant current iL , as shown in Fig. 3. Lower and upper bounds of α are given by

$$0 \le \alpha \le \frac{\pi}{2}. \quad (5)$$

The half-wave cycloconverter behaves as a controlled half-wave rectifier when $\alpha = 0^\circ$. In such a case, the switching sequence of the half-wave cycloconverter is summarized in Table I. The grid-synchronized 50-Hz sinusoidal current can be obtained by varying the switching sequence starting instant with respect to the resonant current.

C. Power Flow Calculation

The ideal waveforms of the microinverter are shown in Fig. 3 by using two assumption made in Section II-A where PV input voltage and grid voltage are considered as constant over one switching period of the microinverter. The resonant current iL of the inverter should lag the full-bridge output vfb to ensure ZVS in the full-bridge inverter, as shown in Fig. 3. Then, the antiparallel diode in the power switch will be turned ON before the power switch, ensuring there will be zero voltage across power switch when it turns ON. On the other hand, the resonant current should lead the cycloconverter input voltage vo fb , in order to ensure ZVS in the half-wave cycloconverter. Also, ZVS turn-on of the cycloconverter depends on the switching sequence of the power switches. u3,L, $\bar{u}$3,H should be completely turned ON when Vo u t>0 and u3,H, $\bar{u}$3,L should be completely turned ON when Vo u t<0 during each switching cycle in order to confirm ZVS in the cycloconverter switches.

The cycloconverter can be represented by using an equivalent single reactive element, as shown in Fig. 4, due to the current lagging operation of the cycloconverter.

The Fourier series expansion of the three stepped voltage v_{fb} is given as

$$v_{fb} = \sum_{i=1,3,5,\ldots}^{\infty} \frac{4V_{in}}{i\pi} \cos\left(\frac{i\theta}{2}\right) \sin(i\omega_s t), \quad i = 1, 3, 5, \ldots. \tag{6}$$

The Fourier series expansion of $v_{o\,fb}$ is given as

$$v_{o\,fb} = \frac{v_{out}}{2} + \sum_{i=1}^{\infty} \frac{2V_{out}}{i\pi} \sin(i\omega_s t - i\phi), \quad i = 1, 3, 5, \ldots. \tag{7}$$

The average output power over one switching cycle of inverter can be calculated using the assumption of constant $V_{o\,fb}$ during one switching cycle. Therefore, the average output power during

$$P_{out} = \frac{1}{2\pi} \int_{\alpha}^{\pi+\alpha} v_{o\,fb}(t) i_{o\,hf}(t) d(\omega_s t)$$

$$P_{out} = \frac{1}{\pi} v_{out} I_{res} \cos(\alpha) \tag{8}$$

where I_{res} is the peak current of $i_{o\,hf}$ and $V_{o\,ut}$ is an instantaneous value of the grid voltage. The average power over one switching cycle can be calculated using root mean square (RMS) of $v_{o\,fb}$ and the equivalent load resistance R_o at a given average power level, as

$$P_{out} = \frac{2}{\pi^2} \frac{V_{out}^2}{R_o}. \tag{9}$$

Therefore, the phase shift α between i_L and $v_{o\,fb}$ can be obtained As

$$\cos\alpha = \angle v_{out}. \tag{10}$$

The total impedance of the cycloconverter can be calculated using the equivalent circuit of the cycloconverter shown in Fig. 4. The complex impedance of the cycloconverter is given as

$$Z = R_x - \frac{j}{\omega C_x}$$

$$|Z| = \frac{\sqrt{(R_x C_x \omega)^2 + 1}}{C_x \omega}$$

$$\tan\alpha = \frac{1}{R_x C_x \omega}. \tag{11}$$

The cycloconverter peak input voltage to peak resonant current ratio can be used to calculate the magnitude of cycloconverter total impedance as

$$|Z| = \frac{2}{\pi} \frac{v_{out}}{I_{res}}. \tag{12}$$

Then, the phase shift α between i_L and $v_{o\,fb}$ can be calculated As

$$\cos\alpha = \frac{\sqrt{(R_x C_x \omega)^2 + 1}}{R_x C_x \omega} \tag{13}$$

where R_x and C_x can be calculated as (14). A similar derivation

can be found in [26] for the microinverter presented in [4]

$$R_x = R_o \cos^2 \alpha$$

$$C_x = \frac{2}{\quad} . \qquad (14)$$

Then, the total resonance capacitance is given as

$$C = \frac{C\,C}{\quad} \qquad (15)$$

where C_x is the primary referred load capacitance, given by $n^2 C_x$. Hence, the quality factor Q of the series-resonant tank is given by (16). The resonant components L and C should be selected appropriately in order to restrict the variation of Q within the acceptable range to ensure sinusoidal current in resonant tank due to variation in α

$$Q = \frac{\sqrt{L/C}}{\frac{}{n^2} R_x} \qquad (16)$$

The harmonics in v_{fb} and $v_{o\,fb}$ can be neglected with the assumption of a high quality factor [27] of the resonant circuit. Therefore, the resonant current i_L is given as follows:

$$i_{L,pu} = \frac{\frac{2M}{\pi}\cos(\omega_s t-\phi) - \frac{4}{\pi}\cos\left(\frac{\theta}{2}\right)\cos(\omega_s t)}{X_r} \qquad (17)$$

where

$$X_r = Q\left(f - \frac{1}{f}\right), \quad M = \frac{v_{out}}{nV_{in}}.$$

Here, $f = \omega_s : \omega_s$ is the switching frequency and ω_r is the resonant frequency. Here, M is defined as the instantaneous voltage gain of the inverter. The power delivered from primary side to secondary side can be obtained as

$$P_{d,pu}(t) = \frac{\frac{2M}{\pi}\cos(\omega_s t-\phi) - \frac{4}{\pi}\cos\left(\frac{\theta}{2}\right)\cos(\omega_s t)}{X_r} \times \pi\cos\frac{2}{4}\sin\frac{\theta}{}(\omega_s t). \qquad (18)$$

Hence, the average power delivered during one switching cycle is given by (19) and can be compared to that given in [28]. According to (19), there are two variables that affect the power delivery in this topology: phase shift ϕ measured between v_{fb} and $v_{o\,fb}$ and the full-bridge phase shift θ

$$P_{d,avg(pu)} = \frac{1}{2\pi}\int_0^{2\pi} P_d(t)\,d(\omega_s t)$$

$$P_{d,avg(pu)} = 4M \sin 2\phi \cos\frac{\theta}{2} \qquad (19)$$

From a design perspective, n is defined as V o u t,m a x/Vin, and then 0 ≤M≤ 1. Hence, during one cycle of the grid voltage, M varies from 0 to 1 and then again to 0. Fig. 5 shows the delivered power from the primary side to the secondary side as a function of phase shift ϕ at different Q values. Fig. 5 shows that the phase shift needed to transfer the power depends on the Q of the series-resonant circuit.

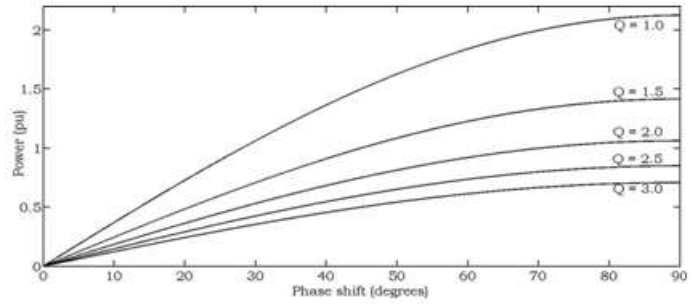

Fig. 5. Delivered power against phase shift ϕ when f= 1.1, M= 1, and θ= 0 at the different Q values.

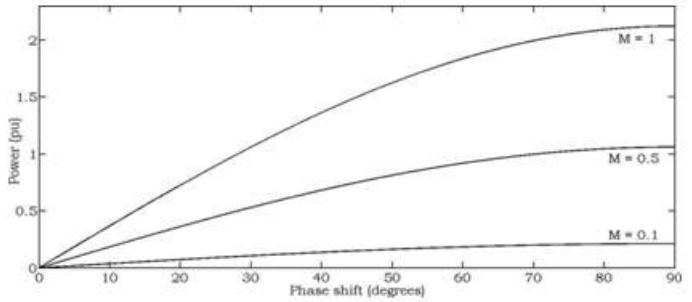

Fig. 6. Delivered power against phase shift ϕ when f= 1.1, Q= 1, and θ= 0 at the different M values.

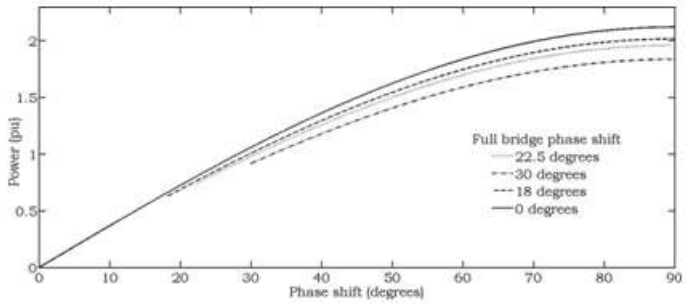

Fig. 7. Delivered power against phase shift ϕ with different values of full-bridge phase shift θ when f= 1.1, Q= 1, and M= 1.

Fig. 6 shows the nonlinear relationship between delivered power and phase shift for the different instantaneous voltage gains of the inverter. According to Fig. 6, the maximum phase shift must be used to deliver full power at the maximum output voltage. The phase shift needed to transfer a given power at a given voltage level of the output voltage (or to have desired voltage gain M) can be obtained using Fig. 6. Similar plots can be used to obtain the required phase shift to deliver a given output power at different full-bridge phase-shift angles θ.

Fig. 7 shows the relationship between the delivered power and the phase shift ϕ of the inverter for different values of full-bridge phase shift θ at the maximum voltage gain of the inverter with Q= 1. The phase shift ϕ should be increased to deliver the given output power with increasing full-bridge phase shift θ. Therefore, the inverter can be designed with a particular full-bridge phase shift θ1 to deliver maximum power at maximum input voltage. Then, the phase shift θ2(< θ1) can be used to obtain the desired power delivery capability at a lower input voltage level.

D. Soft-Switching Principle

A significantly higher switching frequency is used in the pro-posed inverter in order to reduce the size of passive compo-nents. However, switching power losses in the power switches are proportional to the switching frequency. ZVS is proposed as a soft-switching method for this inverter to reduce the switch-ing power losses. The input-side resonant current (17) can be simplified to (20) in order to analyze the resonant current be-havior with respect to the full-bridge output voltage v_{fb} and the cycloconverter input voltage $v_{o\,fb}$

$$i_{L,pu} = \frac{}{4\pi X_r}\ 0.5M\cos(\omega_s t-\phi) - \cos\ \frac{2}{\theta}\ \cos(\omega_s t)\ .$$

(20)

The zero crossing angle β of the resonant current i_L is given by the following equation, as shown in Fig. 3:

$$\beta = \tan^{-1}\ \frac{\cos\ \frac{\vartheta}{2} - 0.5M\cos(\phi)}{0.5M\sin(\phi)}\ . \qquad (21)$$

The full-bridge output voltage v_{fb} should lead the resonant cur-rent in order to ensure ZVS at the four switches in the full-bridge. The soft-switching behavior of input full-bridge can be analyzed by evaluating the resonant current at $\omega_s t=\frac{\vartheta}{2}$. The resonant current at $\omega_s t=\frac{\vartheta}{2}$ is given as

$$i_{L,pu} = \frac{}{4\pi X_r} 0.5M\cos\ \frac{2}{\theta} - \phi\ - \cos\ \frac{2}{\theta}\ \cos\ \frac{2}{\theta}\ .$$

(22)

According to (22), $0.5M\cos(\frac{\vartheta}{2}-\phi)-\cos(\frac{\vartheta}{2})\cos(\frac{\vartheta}{2})\le 0$ in order to have ZVS at the input full-bridge.

Therefore, phase-shift angle combinations of $\frac{\vartheta}{2}$ and ϕ can be found using Fig. 8 and by using the relationship $\frac{\vartheta}{2}\le\beta\le\phi$, where β is given by (21). Fig. 8 shows the feasible operating regions when selecting $\frac{\vartheta}{2}$ and ϕ as the voltage gain is varied. Any phase-shift angle combination can be chosen to give the desired output power at voltage gains less than unity, as long as the $\frac{\vartheta}{2}\le\phi$ condition is satisfied.

It can be further explained by using Fig. 9. It shows the zero crossing angle β of the resonant current i_L at different inverter phase-shift ϕ and full-bridge phase-shift ($\frac{\vartheta}{2}$) angles when the inverter has highest voltage gain (M= 1). If $\frac{\vartheta}{2}$ and ϕ are selected as 15° and 64°, then expected zero crossing angle of the resonant current (β) will be 59°. On the other hand, if $\frac{\vartheta}{2}$ and ϕ are selected as 15° and 75°, then expected β will be 60°. The corresponding β values can be found using a similar method at different M values in order to predict the behavior of the resonant current.

A similar analysis for the resonant current i_L can be un-dertaken to obtain the conditions for ZVS in the cycloconverter switches, as in (23). As the resonant current should lead the volt-age $v_{o\,fb}$ for ZVS in all power switches of the cycloconverter, it follows that $i_L \ge 0$ at $\omega_s t=\phi$

$$\frac{}{4} \qquad \frac{}{\theta}$$

Hence, $M \ge 2\cos\phi\cos\ \frac{\vartheta}{2}$ to satisfy the above condition. But requirement ≤ 1, it is necessary

according to the design M

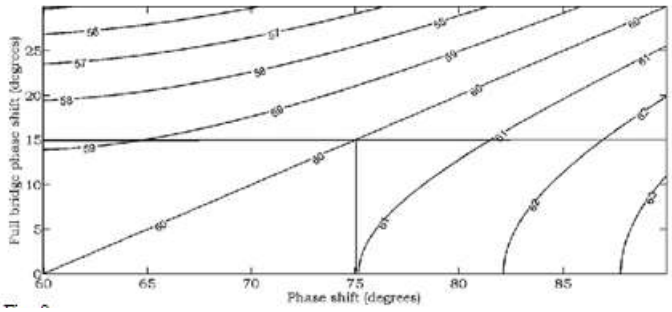

Fig. 9. Contours of zero crossing angle β of the resonant current i_L at different phase-shift ϕ and full-bridge phase shift ($\frac{\vartheta}{2}$) when M= 1.

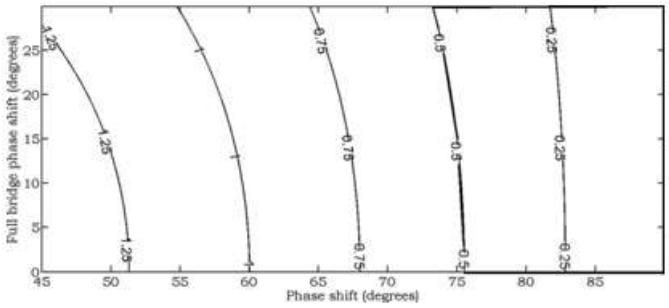

Fig. 10. Contours of $\cos\phi\cos(\frac{\theta}{2})$ against phase-shift ϕ and full-bridge phase shift ($\frac{\theta}{2}$) at f= 1.1 and Q= 1. Feasible operating region is shown by the area enclosed by bold lines

to have $2\cos\phi\cos\frac{\theta}{2}\leq 1$ for ZVS at the cycloconverter, as shown in Fig. 10. According to Fig. 10, it is not possible to have ZVS at every combination of θ and ϕ. So phase-shift combinations need to satisfy conditions $\frac{\theta}{2}\leq\beta\leq\phi$ and $M\geq$
$2\cos\phi\cos\frac{\theta}{2}$ to have ZVS at the half-wave cycloconverter, 2
whereβ is given by (21).

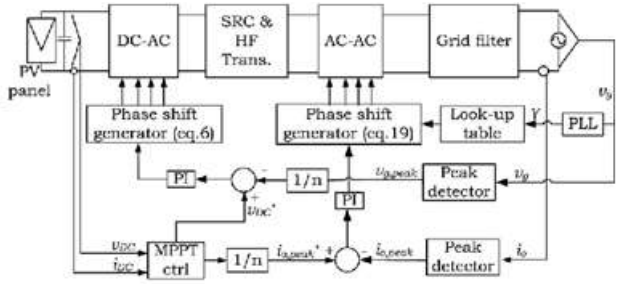

Fig. 11. Overall structure of the microinverter.

Table II: Microinverter Parameters

Parameter	Value
Resonant inductor (L)	$84.60\mu H$
Resonant capacitor (C)	120.9nF
Switching frequency (f_s)	$42.2kHz$
Quality factor (Q)	4
Input voltage (V_{in})	$40V$
RMS output voltage (v_{out})	$230V$
Transformer turns ratio (n)	8

On the other hand, all power switches in the full-bridge are turned OFF with higher currents. Turn-off power losses in the switches can be minimized, adding additional output capaci-tance across each power switch.

III. Simulation And Experimental Verification

A. Proposed Controller

The overall structure of the proposed microinverter is shown in Fig. 11. The microinverter controller has two independent closed loops that control the output current (or power) and the PV-link voltage of the microinverter. The maximum power point (MPP) tracker locates and provides PV MPP voltage and current set point to the respective loop to obtain the desired control. In the current control loop, inverter phase shift ϕ is used to control the output current of the microinverter, as it can be shown from (19) that the current can be effectively regulated by controlling ϕ in the grid-connected mode. ϕ is varied within a specific limitbased on the peak value of the grid current i_o and the refer-ence grid current $i^*_{o,\mathrm{peak}}$. The required ϕ is calculated by the phase-shift controller of the ac–ac converter, using the phase-locked loop output γ as an input, as shown in Fig. 11.

The phase-shift controller can be developed either by using modula-tion methods or using a lookup table. Although the lookup table is proposed as a common ϕ control strategy for similar topolo-gies, in this paper, the required output current is calculated by modulating ϕ using γ. The full-bridge phase shift θ can be used to control the PV-link voltage of the inverter according to (6) and, hence, the operating point of the PV characteristic curve. The MPP tracker output voltage vD∗ C is fed forward to generate a reference for the voltage control loop. All the constraints ob-tained in the Section II-D can be used to decide the allowable phase-shift combinations.

B. Simulation Results

The proposed microinverter is simulated with MATLAB/ Simnulink and PLECS toolboxes to verify its operation. The design objectives of the inverter can be specified as soft switch-ing at the all power switches, reduced resonant component size, and high-efficiency operation. The calculation of resonant com-ponents of the inverter is based on the equations presented in Section II-C. With varying output power, it is difficult to choose the proper resonant component size to allow soft-switching op-eration throughout the whole operational range. Therefore, the average power of the inverter is used to calculate the equivalent load resistance of the inverter. The quality factor Q of the series-resonant circuit is chosen as 4 in order to confirm validity of the sinusoidal approximation. The ratio of switching frequency to resonant frequency f is chosen as 1.1 in order to verify the soft-switching operation of all power switches of the inverter. The required phase shift to obtain the given power output is cal-culated using the equations presented in Section II-C with the constraints obtained in Section II-D. It is observed that the phase shift ϕ required to obtain power variation from full-load to zero load is limited and is approximately 45°. Table II summarizes the parameters used in the simulation.

Fig. 12 shows in-phase grid voltage and current waveforms of the simulated microinverter rated to 278 W and it is evident that used phase-shift modulation and its implementation is viable to use in this topology. Fig. 13(a) shows the full-bridge output v_{fb}, the cycloconverter input $v_{o\,fb}$, and the primary-side resonantcurrent i_L of the inverter at the positive peak of the grid voltage. Fig. 13(a) shows that the resonant current i_L lags the full-bridge output voltage v_{fb} and leads the cycloconverter input $v_{o\,fb}$ and hence verifies that ZVS occurs at all power switches. Fig. 13(b) shows unfiltered current i_{ohf} at the cycloconverter output.

A similar set of waveforms is shown in Fig. 14 at the negative peak of the grid voltage. Fig. 14(a) shows that the full-bridge

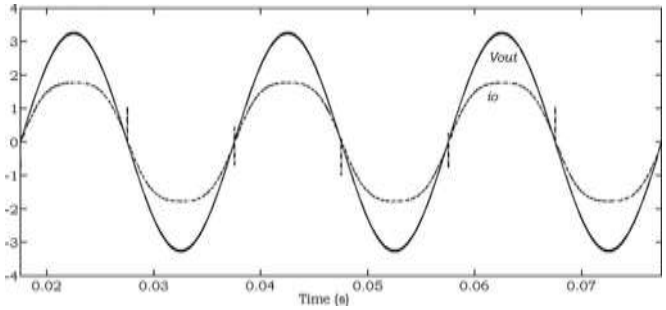

Fig. 12. Output current (A) and scaled (1:100) grid voltage (V) of the inverter.

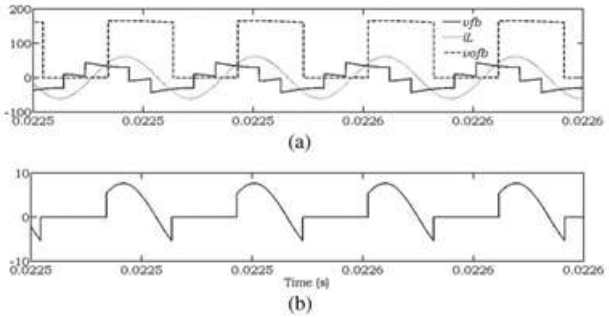

Fig. 13. (a) Simulated resonant current i_L , full-bridge output voltage v_{fb} , and scaled (1:2) cycloconverter input voltage v_{ofb} . (b) Unfiltered output current at the positive peak of the grid voltage v_{out} .

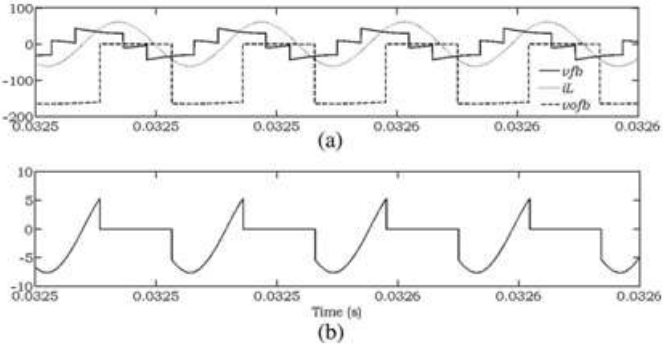

Fig. 14. (a) Simulated resonant current i_L , full-bridge output voltage v_{fb} , and scaled (1:2) cycloconverter input voltage v_{ofb} . (b) Unfiltered output current at the negative peak of the grid voltage v_{out} .

voltage v_{fb} leads the resonant current i_L and hence confirms the soft-switching operation at the input full-bridge. Also, the resonant current i_L leads the cycloconverter input, and hence, there is ZVS in the cycloconverter power switches.

C. Experimental Results

The 100-W microinverter prototype is designed and built in the laboratory for verification purposes. Metal–oxide– semiconductor field-effect transistors (MOSFETs) are used as power switches with appropriate voltage and current ratings. The MOSFET gate drivers are developed using optoisolators and MOSFET gate drive integrated circuits (IC). A TMS320F28335 digital signal processor is used to control the microinverter. The dead bands in the input full-bridge control signals are chosen

Table III: Parameters Of The Experimental Setup

Parameter	Value
Resonant inductor (L)	$14.26\mu H$
Resonant capacitor (C)	$0.69\mu F$
Switching frequency (f_s)	$56.7kHz$
Leakage inductance of transformer primary winding	$0.1\mu H$
Leakage inductance of transformer secondary winding	$23.5\mu H$
Input voltage (V_{in})	$40V$
Transformer turns ratio (n)	8
Output filter capacitor (C_o)	$2\mu F$
Input buffer capacitor (C_{buf})	$8800\mu F$

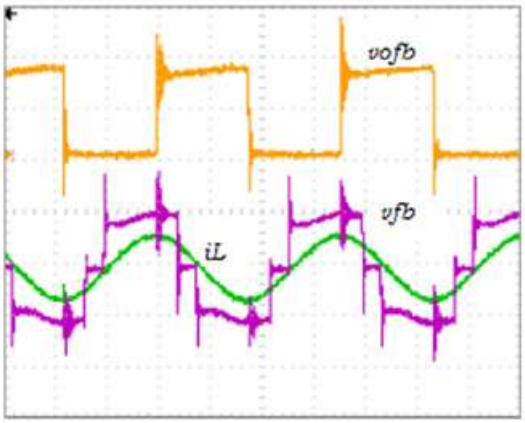

Fig. 16. Full-bridge output voltage v_{fb}, resonant current i_L, and cyclocon-verter input voltage v_{ofb} at $\alpha=\frac{\pi}{2}$ in the positive half cycle of the inverter output

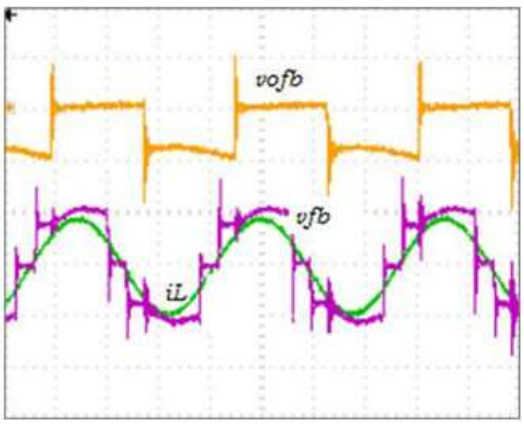

Fig. 17. Full-bridge output voltage v_{fb}, resonant current i_L, and cyclocon-verter input voltage v_{ofb} at $\alpha=\frac{\pi}{8}$ in the negative half cycle of the inverter output.

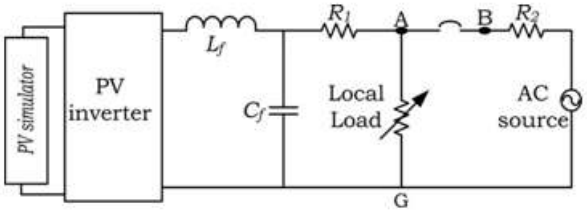

Fig. 18. Setup configuration used to test microinverter connection to an acpowersource

without affecting the intended shape of vfb , in order to prevent possible short-circuit conditions in the input source. Fig. 15 shows the experimental setup of the developed microinverter with grid connection setup. Table III summarizes the circuit parameters of the inverter. The series resonant tank of the mi-croinverter is placed on the primary side of the high-frequency transformer.
expected waveforms to have ZVS at the turn-on of the power switches in the full-bridge inverter and the cycloconverter. But ZVS of the cycloconverter depends on the switching sequence of the power switches, as explained in Section II-C.
The microinverter is tested in grid-connected mode by using the configuration shown in Fig. 20. R1 and R2 are two 3.3-Ω resistors. The voltages at the point of connection (A and B) are shown in Fig. 21, both before and after grid connection. Fig. 21 shows that there is no significant variation in harmonic content of the microinverter output current.

Subsequently, the microinverter is tested at numerous operat-ing points of the PV characteristic curves generated by SAS (a built in program for the solar array simulator by Sandia National Labs) and table modes in the Chroma 62000H programmable dc power supply. for three different PV curves generated according to the parameters given in Table IV. Moreover, the microinverter is tested using table mode of the dc power supply by generating

Table IV: Parameters Of The Pv Curves Generated By Sas Modeof The Solar Array Simulator

Parameter	55%	45%	35%
Open circuit voltage (V_{oc})	24.38V	24.38V	24.38V
Short circuit Current (I_{sc})	3.91A	3.19A	2.13A
Voltage at maximum power (V_{mp})	19V	19V	19V
Current at maximum power (I_{mp})	3.47A	2.842A	1.895A
Maximum power (P_{mp})	66W	54W	36W

an identical set of curves. The results from that test are shown in Fig. 22(b). In both modes, full-bridge phase shift θ is varied from its minimum to maximum value and inverter phase shift ϕ is varied from its minimum to maximum value at each step of θ. Fig. 22 shows that the inverter is able to operate over a range of constant current and constant voltage points as well as at MPP of the tested PV curves.

The maximum power point tracking (MPPT) capability of the microinverter is tested by using the same solar array simulator. The typical PV characteristic curves generated by the solar array simulator mode of the power supply are shown in Fig. 23. The MPP tracker of the inverter is developed by using perturb and observation method (P&O). Peak power of the PV output curve is incremented in 2% intervals from the corresponding value of the lower curve of Fig. 23 to the corresponding value of the upper curve in order to test the MPP tracking capabilityan identical set of curves. The results from that test are shown in Fig. 22(b). In both modes, full-bridge phase shift θ is varied from its minimum to maximum value and inverter phase shift ϕ is varied from its minimum to maximum value at each step of θ. Fig. 22 shows that the inverter is able to operate over a range of constant current and constant voltage points as well as at MPP of the tested PV curves.

The maximum power point tracking (MPPT) capability of the microinverter is tested by using the same solar array simulator. The typical PV characteristic curves generated by the solar array simulator mode of the power supply are shown in Fig. 20. The MPP tracker of the inverter is developed by using perturb and observation method (P&O). Peak power of the PV output curve is incremented in 2% intervals from the corresponding value of the lower curve of Fig. 20 to the corresponding value of the upper curve in order to test the MPP tracking capability.

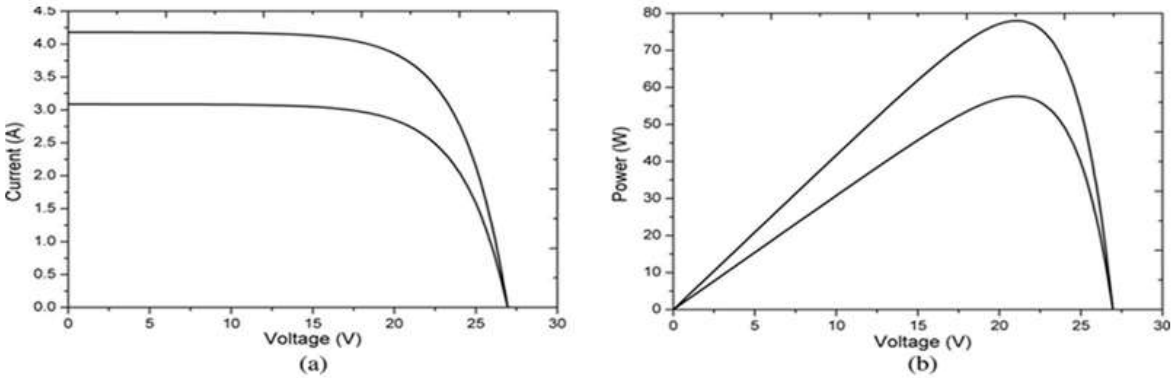

Fig. 20. Tested characteristic curves of the PV model.

IV. Conclusion

A microinverter topology is proposed with a half-wave cy-cloconverter and a full-bridge inverter. There is only one power conversion stage and hence a reduced number of power switches resulting in reduced switching and conduction losses. The trans-former size is reduced because it is placed in the high-frequency link of the inverter resulting in a small and reduced weight sys-tem. The series-resonant tank is used to implement soft switch-ing at the turn-on of the power switches to reduce switching losses due to the increased switching frequency.

The operation of the inverter is critically analyzed and meth-ods are presented to calculate the size of the resonant com-ponents. A relationship between the inverter phase shift, the full-bridge phase shift, the voltage gain of the inverter, the qual-ity factor of the series-resonant tank, and the delivered power is derived. The soft-switching operation of the full-bridge half-wave cycloconverter is analyzed using the derived resonant current equation for the three stepped full-bridge output voltage and the half-wave cycloconverter input voltage. Simulation re-sults are presented to verify the design process and the operation of the inverter. Finally, experimental results are given to further validate the viability of this inverter to be used as an efficient microinverter in PV applications.

References

[1]. A. Zahedi, "Solar photovoltaic (PV) energy; latest developments in the building integrated and hybrid PV systems," Renew. Energy, vol. 31, no. 5, pp.711–718, Apr. 2006.

[2]. R. Teodorescu, M. Liserre, and P. Rodr´ıguez, Grid Converters for Photo-voltaic and Wind Power Systems. New York: Wiley, 2010.

[3]. L. Zhang, K. Sun, Y. Xing, L. Feng, and H. Ge, "A modular grid-connected photovoltaic generation system based on DC bus," IEEE Trans. Power Electron., vol. 26, no. 2, pp. 523–531, Feb. 2011.

[4]. A. Trubitsyn, B. Pierquet, A. Hayman, G. Gamache, C. Sullivan, and D. Perreault, "High-efficiency inverter for photovoltaic applications," in Proc. IEEE Energy Convers. Congr.Expo., Sep. 2010, vol. 1, pp. 2803– 2810.

[5]. H. Krishnaswami, "Photovoltaic microinverter using single-stage isolated high-frequency link series resonant topology," in Proc. IEEE Energy Con-vers. Congr.Expo., Sep. 2011, vol. 1, no. 1, pp. 495–500.

[6]. T. Shimizu and K. Wada, "Flyback-type single-phase utility interactive inverter with power pulsation decoupling on the dc input for an ac pho-tovoltaic module system," IEEE Trans. Power Electron., vol. 21, no. 5, pp. 1264–1272, Sep. 2006.

[7]. H. Patel and V. Agarwal, "A single-stage single-phase transformer-less doubly grounded grid-connected PV interface," IEEE Trans. Energy Con-vers., vol. 24, no. 1, pp. 93–101, Mar. 2009.

[8]. S. Funabiki and T. Tanaka, "A new buck-boost-operation-based sinusoidal inverter circuit," in Proc. IEEE Power Electron. Spec. Conf., 2002, vol. 4, pp. 1624–1629.

[9]. W. Yu, J. S. Lai, H. Qian, and C. Hutchens, "High-efficiency MOSFET in-verter with H6-type configuration for photovoltaic nonisolated ac-module applications," IEEE Trans. Power Electron., vol. 26, no. 4, pp. 1253–1260, Apr. 2011.

[10]. D. Cao, S. Jiang, and X. Yu, "Low-cost semi-z-source inverter for single-phase," IEEE Trans. Power Electron., vol. 26, no. 12, pp. 3514–3523, Dec. 2011.

[11]. B. Yang, W. Li, Y. Gu, W. Cui, and X. He, "Improved transformerless inverter with common-mode leakage current elimination for a photovoltaic grid-connected power system," IEEE Trans. Power Electron., vol. 27, no. 2, pp. 752–762, Feb. 2012.